8220 *Inorg. Chem.* **2009**, *48*, 8220–8226
DOI: 10.1021/ic9006873

Inorganic Chemistry
Article

Crystal Growth, Structural Properties, and Photophysical Characterization of $Ln_4Na_2K_2M_2O_{13}$ (M = Nb, Ta; Ln = Nd, Sm, Eu, Gd)

Thomas-C. Jagau, Irina P. Roof, Mark D. Smith, and Hans-Conrad zur Loye*

Chemistry and Biochemistry, University of South Carolina, Columbia, South Carolina 29208

Received April 8, 2009

Single crystals of $Ln_4Na_2K_2M_2O_{13}$ (Ln = Nd, Sm, Eu, Gd; M = Nb, Ta) were grown out of a reactive high temperature hydroxide melt. The structures were determined by single crystal X-ray diffraction. $Ln_4Na_2K_2M_2O_{13}$ crystallizes in the monoclinic space group $C2/c$ in which niobium and tantalum are located in a rare 5-coordinate, square pyramidal coordination environment. Optical band gaps were estimated from diffuse reflectance UV/vis spectra. The magnetic susceptibility data were measured, and the intense room temperature photoluminescence of the europium containing compounds was studied.

Introduction

Complex niobium and tantalum containing oxides have been of interest for their photocatalytic activity,[1−5] their photoluminescence,[6−14] and their high dielectric constants.[15,16] Possible applications in the fields of photocatalytic splitting of water and microwave dielectric resonators have provided the driving force for the search for new ternary and quaternary niobium and tantalum oxides. In addition, the luminescent properties of such oxides have been investigated, mostly in compositions doped with rare earth ions because of the likely f-f transitions and f-d transitions.[8,10,12] All of the above properties of course strongly depend on the specific electronic and, therefore, crystal structure of the material, fueling the interest to pursue the discovery of new niobates and tantalates.

Many such investigations have focused on complex layered niobates and tantalates containing niobium or tantalum in octahedral coordination environments,[17,18] as only a few compounds with other coordination environments, such as square pyramidal, are known.[19−22] It is believed that the octahedral coordination environment of niobium or tantalum within a complex structure is responsible for the diverse properties of the material.[1,5,23] However, there have been some reports on materials containing niobium or tantalum in a rare square pyramidal coordination environment, as found in $Rb_4Nb_6O_{17}$,[20] LnRbNaMO$_5$ (Ln = La, Nd, Sm, Eu, Gd; M = Nb, Ta),[22] Ln_2KNbO$_6$ (Ln = La, Nd),[13] LaKNaNbO$_5$,[21] EuKNaTaO$_5$,[24] and LnKNaNbO$_5$ (Ln = La, Pr, Nd, Sm, Eu, Gd, and Tb).[19] The title compounds are structurally closely related to LnKNaMO$_5$. One member of the series of oxides discussed herein, $Gd_4Na_2K_2Nb_2O_{13}$, had already been reported by Liao and Tsai,[21] prompting us to concentrate our

*To whom correspondence should be addressed. E-mail: zurloye@mail.chem.sc.edu. Phone: +1-803-777-6916. Fax: +1-803-777-8508.

(1) (a) Machida, M.; Yabunaka, J.; Kijima, T. *Chem. Mater.* **2000**, *12*, 812–817. (b) Nyman, M.; Rodriguez, M. A.; Alain, T. M.; Anderson, T. M.; Ambrosini, A. *Chem. Mater.* **2009**, *21*, 2201–2208.
(2) Abe, R.; Higashi, M.; Zou, Z.; Sayama, K.; Abe, Y.; Arakava, H. *J. Phys. Chem. B* **2004**, *108*, 811–814.
(3) Shimizu, K.; Tsuji, Y.; Hatamachi, T.; Toda, J.; Kodama, T.; Sat, M.; Kitayama, Y. *Phys. Chem. Chem. Phys.* **2004**, *6*, 1064–1069.
(4) Zhang, G.; Zou, X.; Gong, J.; He, F.; Zhang, H.; Zhang, Q.; Liu, Y.; Yang, X.; Hu, B. *J. Alloys Compd.* **2006**, *425*, 76–80.
(5) Liu, J. W.; Chen, G.; Li, Z. H.; Zhang, Z. G. *Int. J. Hydrogen Energy* **2007**, *32*, 2269–2272.
(6) Srivastava, A. M.; Ackermann, J. F.; Beers, W. W. *J. Solid State Chem.* **1997**, *134*, 187–191.
(7) Kudo, A.; Shibata, T.; Kato, H. *Chem. Lett.* **1999**, *9*, 959–960.
(8) Yu, C. C.; Liu, X. M.; Yu, M.; Liu, C. K.; Li, C. X.; Wang, H.; Liu, J. *J. Solid State Chem.* **2007**, *180*, 3058–3065.
(9) Zhou, Y.; Lu, M.; Qin, Z.; Zhang, A.; Ma, Q.; Zhang, H.; Yang, Z. *Mater. Sci. Eng., B* **2007**, *140*, 128–131.
(10) Liu, B.; Han, K.; Liu, X.; Gu, M.; Huang, S.; Ni, C.; Qi, Z.; Zhang, G. *Solid State Commun.* **2007**, *144*, 484–487.
(11) Liu, X. M.; Liu, J. *J. Lumin.* **2007**, *122*−*123*, 700–703.
(12) Wen, C. H.; Chu, S. Y.; Shin, Y. Y.; Lee, C. T.; Juang, Y. D. *J. Alloys Compd.* **2008**, *459*, 107–112.
(13) Roof, I. P.; Park, S.; Vogt, T.; Rassolov, V.; Smith, M. D.; Omar, S.; Nino, J.; zur Loye, H.-C. *Chem. Mater.* **2008**, *20*, 3327–3335.
(14) Gasparotto, G.; Lima, S. A. M.; Davolos, M. R.; Varela, J. A.; Longo, E.; Zaghete, M. A. *J. Lumin.* **2008**, *128*, 1606–1610.
(15) Thirumal, M.; Jain, P.; Ganguli, A. K. *Mater. Chem. Phys.* **2001**, *70*, 7–11.
(16) Solomon, S.; Joseph, J. T.; Kumar, H. P.; Thomas, J. K. *Mater. Lett.* **2006**, *60*, 2814–2818.
(17) Zhang, G.; He, F.; Zou, X.; Gong, J.; Zhang, H.; Zhang, Q.; Liu, Y. *J. Alloys Compd.* **2007**, *425*, 82.
(18) Liu, J. W.; Chen, G.; Li, Z. H.; Zhang, Z. G. *Int. J. Hydrogen Energy* **2007**, *32*, 2269.
(19) Roof, I. P.; Jagau, T.-C.; Zeier, W. G.; Smith, M. D.; zur Loye, H.-C. *Chem. Mater.* **2008**, *21*(9), 1955–1961.
(20) Serafin, M.; Hoppe, R. *Rev. Chim. Mineral.* **1983**, *20*, 214–218.
(21) Liao, J.-H.; Tsai, M.-C. *Cryst. Growth Des.* **2002**, *2*, 83–85.
(22) Cavazos, R. J.; Schaak, R. E. *Mater. Res. Bull.* **2004**, *39*, 1209–1214.
(23) Roof, I. P.; Smith, M. D.; zur Loye, H.-C. *J. Cryst. Growth* **2008**, *310*, 240–244.
(24) Roof, I. P.; Smith, M. D.; Park, S.; zur Loye, H.-C. *J. Am. Chem. Soc.* **2009**, *131*, 4202.

Published on Web 07/30/2009

Table 1. Crystal Data and Structural Refinement for $Ln_4K_2Na_2Nb_2O_{13}$

empirical formula	$Nd_4K_2Na_2Nb_2O_{13}$	$Sm_4K_2Na_2Nb_2O_{13}$	$Eu_4K_2Na_2Nb_2O_{13}$	$Gd_4K_2Na_2Nb_2O_{13}$
formula weight (g/mol)	1094.96	1119.40	1125.84	1147.00
space group	$C2/c$	$C2/c$	$C2/c$	$C2/c$
a (Å)	24.3144(9)	24.1511(6)	24.093(4)	24.030(2)
b (Å)	5.7255(2)	5.6768(1)	5.6581(11)	5.6467(6)
c (Å)	11.3320(4)	11.2319(3)	11.198(2)	11.1706(11)
β (deg)	116.734(1)	116.555(1)	116.495(3)	116.422(1)
V (Å^3)	1408.92(9)	1377.45(6)	1366.2(4)	1356.5(2)
Z	4	4	4	4
density (calculated) (Mg/m^3)	5.162	5.398	5.474	5.617
absorption coefficient (mm^{-1})	16.755	19.112	20.441	21.649
F(000)	1944	1976	1992	2008
crystal size (mm^3)	0.05 × 0.04 × 0.02	0.06 × 0.06 × 0.02	0.07 × 0.05 × 0.02	0.07 × 0.06 × 0.04
Θ range	1.88°—35.12°	1.89°—35.61°	1.89°—35.25°	1.89°—35.22°
reflections collected	16133	15625	15112, 14925 [a]	15990, 16020 [a]
independent reflections	3137 (R_{int} = 0.0606)	3181 (R_{int} = 0.0430)	4109 (R_{int} = 0.0704)	3613 (R_{int} = 0.0696)
reflections used for unit cell parameters	3399	4694	1757	3162
completeness to Θ_{max}	99.8%	99.7%	99.8%	99.8%
goodness-of-fit on F^2	1.018	1.027	1.033	0.969
R indices (all data)	R_1 = 0.0561	R_1 = 0.0390	R_1 = 0.0617	R_1 = 0.0487
	wR_2 = 0.0633	wR_2 = 0.0586	wR_2 = 0.0869	wR_2 = 0.0750
largest diffraction peak and hole(e$^-$/Å^3)	1.858 and −1.751	2.792 and −1.699	3.684 and −2.249	3.603 and −2.525

[a] Twinned crystals. The two values represent reflections from the two twin domains.

synthetic efforts on incorporating additional rare earth elements into the structure, as well as on expanding the known chemistry to include the tantalates.

Most of the known ternary and quaternary niobium and tantalum oxides have been synthesized by traditional solid state techniques, which typically result in the thermodynamically most stable material.[1−4,16,22] Hence, to discover new phases that are only accessible in a lower temperature regime, other synthetic approaches had to be chosen.[13,15,21,23] Specifically, crystal growth out of molten hydroxides, an effective method for the discovery of new oxide materials,[23,25−28] was used to prepare the new niobium and tantalum oxide materials discussed herein.

Hydroxide melts are believed to be one of the best solvent systems for metal oxides, and their dissolution is a necessary step for incorporating metal cations into a crystal. The acid−base chemistry of such a melt is best described by the Lux−Flood concept of oxoacidity.[29,30] On the basis of this concept, the autodissociation of molten hydroxides and the analogous autodissociation of water yields the following equations:

$$2H_2O \rightleftarrows H_3O^+ + OH^- \quad (1)$$

$$2OH^- \rightleftarrows H_2O + O^{2-} \quad (2)$$

Thus, by analogy with water, where H_3O^+ is the acid and OH^- is the base, in a hydroxide melt H_2O is the acid and O^{2-} is the base. The solubility of metal cations in molten hydroxides strongly depends on the melt's acidity.[28] Therefore, the water content of the reaction mixture has to be adjusted to control the solubility of the reagents and, thereby, to influence the crystal growth of complex oxides.[31]

Table 2. Crystal Data and Structural Refinement for $Ln_4K_2Na_2Ta_2O_{13}$

empirical formula	$Sm_4K_2Na_2Ta_2O_{13}$	$Eu_4K_2Na_2Ta_2O_{13}$
formula weight (g/mol)	1295.48	1301.92
space group	$C2/c$	$C2/c$
a (Å)	24.1867(17)	24.1177(7)
b (Å)	5.6795(4)	5.6600(2)
c (Å)	11.2396(8)	11.2030(3)
β (deg)	116.520(2)	116.4300(10)
V (Å^3)	1381.51(17)	1369.44(7)
Z	4	4
density (calculated) (Mg/m^3)	6.229	6.315
absorption coefficient (mm^{-1})	33.226	34.687
F(000)	2232	2248
crystal size (mm^3)	0.07 × 0.04 × 0.02	0.08 × 0.04 × 0.02
Θ range	1.88°—35.29°	1.89°—35.19°
reflections collected	16623	17454
independent reflections	3109 (R_{int} = 0.0674)	3049 (R_{int} = 0.0634)
reflections used for unit cell parameters	2759	3371
completeness to Θ_{max}	99.9%	99.9%
goodness-of-fit on F^2	1.002	1.031
R indices (all data)	R_1 = 0.0577	R_1 = 0.0561
	wR_2 = 0.0717	wR_2 = 0.0683
largest diffraction peak and hole(e$^-$/Å^3)	3.168 and −2.292	2.671 and −2.798

Using a dry alkali hydroxide melt we successfully synthesized a new series of lanthanide containing complex niobates and tantalates, $Ln_4Na_2K_2M_2O_{13}$ (M = Nb, Ta; Ln = Nd, Sm, Eu, Gd). Herein we report the crystal growth, the structure determination, and the magnetic and optical properties of the members of this new series.

Experimental Section

Sample Preparation. Single crystals of $Ln_4Na_2K_2M_2O_{13}$ (M = Nb, Ta; Ln = Nd, Sm, Eu, Gd) were grown out of a sodium and potassium hydroxide flux. In a typical procedure, 1.0 mmol of

(25) Davis, M. J.; Mugavero, S. J. III; Glab, K. I.; Smith, M. D.; zur Loye, H.-C. *Solid State Sci.* **2004**, *6*, 413–417.
(26) Mugavero, S. J. III; Smith, M. D.; zur Loye, H.-C. *J. Solid State Chem.* **2005**, *178*, 200–206.
(27) Gemmill, W. R.; Smith, M. D.; zur Loye, H.-C. *J. Solid State Chem.* **2006**, *179*, 1750–1756.
(28) Mugavero, S. J. III; Gemmill, W. R.; Roof, I. P.; zur Loye, H.-C. *J. Solid State Chem.* **2009**, *182*, 1950–1963.
(29) Lux, H. Z.; Elektrochem, Z. *Angew. Phys. Chem.* **1939**, *45*, 303–309.
(30) Flood, H.; Forland, T. *Acta Chem. Scand.* **1947**, *1*, 592–604.
(31) Keller, S. W.; Carlson, V. A.; Sandford, D.; Stenzel, F.; Stacy, A. M.; Kwei, G. H.; Alario-Franco, M. *J. Am. Chem. Soc.* **1994**, *116*, 8070–8076.

Table 3. Atomic Coordinates and Equivalent Displacement Parameters U_{eq} (Å^2) for $Ln_4K_2Na_2Nb_2O_{13}$[a]

	X	Y	Z	U_{eq}
		$Nd_4K_2Na_2Nb_2O_{13}$		
Nd(1)	0.4363(1)	0.0430(1)	0.5500(1)	0.007(1)
Nd(2)	0.0637(1)	0.0346(1)	0.1745(1)	0.008(1)
Nb(1)	0.3476(1)	0.0321(1)	0.2161(1)	0.007(1)
K(1)	0.2506(1)	0.0503(2)	0.3666(1)	0.019(1)
Na(1)	0.1594(1)	0.0349(4)	0.0245(2)	0.011(1)
O(1)	0.3662(2)	0.2699(6)	0.3563(3)	0.009(1)
O(2)	0.3638(2)	0.2236(6)	0.6228(3)	0.011(1)
O(3)	0.1323(2)	0.3103(6)	0.1409(3)	0.010(1)
O(4)	0.2642(2)	0.0623(7)	0.1226(4)	0.014(1)
O(5)	0	0.2417(9)	1/4	0.012(1)
O(6)	0.3962(2)	−0.2288(6)	0.6575(3)	0.010(1)
O(7)	0.5014(2)	0.2519(6)	0.4771(3)	0.011(1)
		$Sm_4K_2Na_2Nb_2O_{13}$		
Sm(1)	0.4371(1)	0.0437(1)	0.5509(1)	0.008(1)
Sm(2)	0.0629(1)	0.0347(1)	0.1733(1)	0.008(1)
Nb(1)	0.3487(1)	0.0333(1)	0.2173(1)	0.007(1)
K(1)	0.2506(1)	0.0520(2)	0.3664(1)	0.020(1)
Na(1)	0.1591(1)	0.0375(3)	0.0235(2)	0.011(1)
O(1)	0.3672(1)	0.2749(5)	0.3572(3)	0.011(1)
O(2)	0.3652(1)	0.2238(5)	0.6230(3)	0.011(1)
O(3)	0.1311(1)	0.3100(5)	0.1393(3)	0.010(1)
O(4)	0.2649(1)	0.0637(5)	0.1239(3)	0.014(1)
O(5)	0	0.2430(7)	1/4	0.010(1)
O(6)	0.3984(1)	−0.2285(5)	0.6593(3)	0.010(1)
O(7)	0.5009(1)	0.2506(5)	0.4769(3)	0.009(1)
		$Eu_4K_2Na_2Nb_2O_{13}$		
Eu(1)	0.4373(1)	0.0444(1)	0.5510(1)	0.008(1)
Eu(2)	0.0626(1)	0.0351(1)	0.1730(1)	0.008(1)
Nb(1)	0.3492(1)	0.0341(1)	0.2177(1)	0.008(1)
K(1)	0.2506(1)	0.0531(3)	0.3663(2)	0.019(1)
Na(1)	0.1585(1)	0.0390(4)	0.0226(3)	0.010(1)
O(1)	0.3675(2)	0.2757(8)	0.3584(4)	0.011(1)
O(2)	0.3653(2)	0.2242(8)	0.6233(4)	0.011(1)
O(3)	0.1305(2)	0.3109(8)	0.1386(4)	0.010(1)
O(4)	0.2652(2)	0.0644(8)	0.1240(5)	0.014(1)
O(5)	0	0.2416(12)	1/4	0.012(1)
O(6)	0.3994(2)	−0.2296(8)	0.6595(4)	0.012(1)
O(7)	0.5009(2)	0.2523(8)	0.4764(4)	0.009(1)
		$Gd_4K_2Na_2Nb_2O_{13}$		
Gd(1)	0.4374(1)	0.0453(1)	0.5507(1)	0.009(1)
Gd(2)	0.0624(1)	0.0362(1)	0.1721(1)	0.009(1)
Nb(1)	0.3497(1)	0.0349(1)	0.2180(1)	0.009(1)
K(1)	0.2505(1)	0.0548(2)	0.3664(2)	0.020(1)
Na(1)	0.1588(1)	0.0392(4)	0.0225(2)	0.012(1)
O(1)	0.3681(2)	0.2757(8)	0.3598(4)	0.011(1)
O(2)	0.3651(2)	0.2251(8)	0.6232(4)	0.012(1)
O(3)	0.1297(2)	0.3116(8)	0.1373(4)	0.012(1)
O(4)	0.2654(2)	0.0671(7)	0.1244(5)	0.014(1)
O(5)	0	0.2416(13)	1/4	0.012(1)
O(6)	0.4006(2)	−0.2302(8)	0.6619(4)	0.012(1)
O(7)	0.5010(2)	0.2514(8)	0.4765(4)	0.010(1)

[a] U_{eq} is defined as one third of the trace of the orthogonalized U^{ij} tensor.

Table 4. Atomic Coordinates and Equivalent Displacement Parameters U_{eq} (Å^2) for $Ln_4K_2Na_2Ta_2O_{13}$[a]

	X	Y	Z	U_{eq}
		$Sm_4K_2Na_2Ta_2O_{13}$		
Sm(1)	0.4371(1)	0.0438(1)	0.5510(1)	0.0007(1)
Sm(2)	0.0628(1)	0.0349(1)	0.1733(1)	0.0007(1)
Ta(1)	0.3490(1)	0.0334(1)	0.2177(1)	0.0007(1)
K(1)	0.2508(1)	0.0515(3)	0.3671(2)	0.0019(1)
Na(1)	0.1592(1)	0.0367(5)	0.0237(3)	0.0011(1)
O(1)	0.3675(2)	0.2747(8)	0.3577(5)	0.0009(1)
O(2)	0.3646(2)	0.2241(9)	0.6223(5)	0.0011(1)
O(3)	0.1311(2)	0.3096(9)	0.1386(5)	0.0010(1)
O(4)	0.2650(2)	0.0620(10)	0.1241(6)	0.0016(1)
O(5)	0	0.2415(13)	1/4	0.0011(1)
O(6)	0.3987(2)	−0.2299(9)	0.6596(5)	0.0010(1)
O(7)	0.5012(2)	0.2511(8)	0.4770(5)	0.0008(1)
		$Eu_4K_2Na_2Ta_2O_{13}$		
Eu(1)	0.4374(1)	0.0444(1)	0.5510(1)	0.0007(1)
Eu(2)	0.0624(1)	0.0352(1)	0.1728(1)	0.0008(1)
Ta(1)	0.3495(1)	0.0340(1)	0.2182(1)	0.0007(1)
K(1)	0.2506(1)	0.0522(3)	0.3668(2)	0.0019(1)
Na(1)	0.1594(1)	0.0374(5)	0.0239(3)	0.0011(1)
O(1)	0.3680(2)	0.2749(8)	0.3583(5)	0.0010(1)
O(2)	0.3652(2)	0.2260(8)	0.6229(5)	0.0010(1)
O(3)	0.1302(2)	0.3098(8)	0.1377(5)	0.0010(1)
O(4)	0.2653(2)	0.0625(9)	0.1247(5)	0.0014(1)
O(5)	0	0.2425(12)	1/4	0.0010(1)
O(6)	0.3994(2)	−0.2304(8)	0.6601(5)	0.0009(1)
O(7)	0.5009(2)	0.2504(8)	0.4772(5)	0.0011(1)

[a] U_{eq} is defined as one third of the trace of the orthogonalized U^{ij} tensor.

Ln_2O_3 (Alfa Aesar REacton, 99.9%, prefired at 1000 °C for 24 h), 0.5 mmol of M_2O_5 (Alfa Aesar Puratronic, 99.9985%), 2.0 g of NaOH (Fisher, ACS reagent, containing approximately 15% water by weight), and 6.0 g (Ln = Nd, Sm, Eu) or 2.8 g (Ln = Gd), respectively, of KOH (Mallinckrodt Chemicals, containing approximately 15% water by weight) were placed together into a silver crucible. For the preparation of $Gd_4Na_2K_2M_2O_{13}$, $Eu_4Na_2K_2M_2O_{13}$, and $Sm_4Na_2K_2M_2O_{13}$ the system was heated to 450 at 10 °C/min, held at the target temperature for 12 h and then cooled to 350 °C within 1 h. At this point the furnace was shut off and allowed to cool to room temperature. For $Nd_4Na_2K_2Nb_2O_{13}$, in contrast, the system was held only for 2 h at 450 °C after which time the furnace was cooled to 350 °C over 48 h and then held at this temperature for another 1 h. After that time the system was cooled to room temperature by shutting off the furnace. The flux was dissolved in water aided by the process of sonication, and the crystals were collected by filtration. These reaction conditions led to the formation of pure single crystal samples of the desired phases, apart from $Nd_4Na_2K_2Nb_2O_{13}$, which was only obtainable as a mixture with $NdKNaNbO_5$. The application of higher reaction temperatures or longer reaction times leads to the formation of the LnKNaMO$_5$ (M = Nb, Ta) phases.

All crystals were colorless, except for $Nd_4Na_2K_2Nb_2O_{13}$, which was distinctly blue. All our attempts to obtain single crystals of $Nd_4Na_2K_2Ta_2O_{13}$ and $Gd_4Na_2K_2Ta_2O_{13}$ large enough for a structure determination, or to incorporate lanthanides larger than neodymium or smaller than gadolinium into the structure were unsuccessful. Furthermore, our attempts to prepare pure compounds of the series $Ln_4Na_2K_2M_2O_{13}$ by the classical solid-state synthesis were unsuccessful.

Single Crystal X-ray Diffraction. X-ray diffraction intensity data from plate crystals were measured at 294(2) K on a Bruker SMART APEX diffractometer[32] (Mo Kα radiation, λ = 0.71073 Å). The raw area detector data frames were processed with SAINT+.[32] An absorption correction based on the redundancy of equivalent reflections was applied to the data with SADABS.[32] The reported unit cell parameters were determined by least-squares refinement of a large array of reflections taken from each data set (Table 1). Difference Fourier calculations and full-matrix least-squares refinement against F^2 were performed with SHELXTL.[33]

(32) *SMART V. 5.625, SAINT+ V. 6.45, and SADABS V. 2.05*; Bruker Analytical X-ray Systems, Inc.: Madison, WI, 2001.

(33) *SHELXTL V. 6.14*; Bruker Analytical X-ray Systems, Inc.: Madison, WI, 2000.

Table 5. Selected Interatomic Distances (Å) for $Ln_4Na_2K_2Nb_2O_{13}$

	$Nd_4K_2Na_2Nb_2O_{13}$	$Sm_4K_2Na_2Nb_2O_{13}$	$Eu_4K_2Na_2Nb_2O_{13}$	$Gd_4K_2Na_2Nb_2O_{13}$
Ln(1)−O(1)	2.459(3)	2.454(3)	2.440(5)	2.419(4)
Ln(1)−O(2)	2.483(4)	2.445(3)	2.439(4)	2.440(4)
Ln(1)−O(3)^{iii}	2.447(4)	2.427(3)	2.413(5)	2.395(4)
Ln(1)−O(5)^{ii}	2.428(3)	2.396(2)	2.390(4)	2.384(4)
Ln(1)−O(6)	2.434(3)	2.400(3)	2.388(4)	2.392(4)
Ln(1)−O(7)	2.407(4)	2.364(3)	2.360(4)	2.345(4)
Ln(1)−O(7)^{i}	2.379(4)	2.357(3)	2.353(4)	2.343(4)
Ln(2)−O(1)^{iii}	2.421(3)	2.380(3)	2.376(4)	2.368(4)
Ln(2)−O(2)^{ii}	2.580(4)	2.565(3)	2.558(5)	2.556(4)
Ln(2)−O(3)	2.449(4)	2.422(3)	2.414(4)	2.396(5)
Ln(2)−O(5)	2.393(3)	2.370(2)	2.354(3)	2.347(4)
Ln(2)−O(6)^{vii}	2.443(3)	2.420(3)	2.411(4)	2.396(4)
Ln(2)−O(7)^{iii}	2.372(4)	2.344(3)	2.327(5)	2.325(5)
Ln(2)−O(7)^{vi}	2.397(3)	2.375(3)	2.363(4)	2.349(4)
Nb(1)−O(1)	1.984(3)	1.980(3)	1.981(4)	1.981(4)
Nb(1)−O(2)^{viii}	1.948(3)	1.945(3)	1.942(4)	1.940(4)
Nb(1)−O(3)^{iii}	1.941(3)	1.933(3)	1.929(4)	1.932(4)
Nb(1)−O(4)	1.826(4)	1.825(3)	1.827(5)	1.828(4)
Nb(1)−O(6)^{viii}	1.952(4)	1.947(3)	1.952(5)	1.946(4)
K(1)−O(1)	3.129(4)	3.130(3)	3.122(5)	3.119(5)
K(1)−O(1)^{iii}	3.250(4)	3.238(3)	3.241(5)	3.253(5)
K(1)−O(2)	3.131(4)	3.128(3)	3.124(5)	3.116(4)
K(1)−O(2)^{ii}	3.118(4)	3.122(3)	3.113(5)	3.094(4)
K(1)−O(3)	3.226(4)	3.225(3)	3.228(5)	3.235(5)
K(1)−O(3)^{iii}	3.197(4)	3.196(3)	3.197(5)	3.206(5)
K(1)−O(4)	2.930(4)	2.895(3)	2.888(5)	2.881(5)
K(1)−O(4)^{iii}	2.826(4)	2.806(3)	2.800(5)	2.787(4)
K(1)−O(4)^{iv}	2.842(4)	2.833(3)	2.826(5)	2.827(5)
K(1)−O(4)^{v}	2.963(4)	2.937(3)	2.926(5)	2.924(4)
Na(1)−O(1)^{iii}	2.296(4)	2.276(3)	2.264(5)	2.262(5)
Na(1)−O(2)^{iii}	2.331(4)	2.315(3)	2.310(5)	2.299(5)
Na(1)−O(3)	2.332(4)	2.308(3)	2.299(5)	2.302(5)
Na(1)−O(4)	2.281(4)	2.291(4)	2.306(6)	2.300(5)
Na(1)−O(6)^{v}	2.324(4)	2.314(3)	2.298(5)	2.315(5)

^{i}Symmetry code: $-x+1,-y,-z+1$ ^{ii}Symmetry code: $-x+1/2,-y+1/2,-z+1$ ^{iii}Symmetry code: $-x+1/2,y-1/2,-z+1/2$ ^{iv}Symmetry code: $x,-y,z+1/2$ ^{v}Symmetry code: $-x+1/2,y+1/2,-z+1/2$ ^{vi}Symmetry code: $x-1/2,-y+1/2,z-1/2$ ^{vii}Symmetry code: $-x+1/2,-y-1/2,-z+1$ ^{viii}Symmetry code: $x,-y,z-1/2$.

All compounds of the series $Ln_4Na_2K_2M_2O_{13}$ are isostructural and crystallize in the space group $C2/c$. Refinements converged rapidly. There are five metal atom and seven oxygen atom positions in the asymmetrical unit. All atoms are located on general positions except O(5) which is located on a 2-fold rotational axis (Wyckoff site 4e). All atoms were refined with anisotropic displacement parameters. Trial refinements of site occupancy parameters showed no deviation from unity occupancy for the metal atoms. The most important crystallographic data for the niobates and tantalates are summarized in Tables 1 and 2, respectively. Atomic positions and selected interatomic distances are listed in Tables 3, 4, 5 and 6.

UV−vis Spectroscopy. Diffuse-reflectance spectra of ground crystals of all compounds of the series $Ln_4Na_2K_2M_2O_{13}$ were obtained using a PerkinElmer Lambda 35 UV/vis Scanning Spectrophotometer equipped with an integrating sphere. The spectra were converted from reflection to absorbance using the Kubelka−Munk method. The onset of absorption was determined by extrapolating the linear part of the rising curve to zero and used for the reported band gap energies.

Magnetic Susceptibility. The magnetic susceptibility of the compounds $Ln_4Na_2K_2M_2O_{13}$ (Ln = Nd, Sm, Eu, Gd; M = Nb, Ta) was measured using a Quantum Design MPMS XL SQUID magnetometer. For the magnetic measurements, loose crystals of each oxide were placed into a gelatin capsule, which was placed inside a plastic straw. For all compounds, the magnetization was measured in the temperature range of 5−300 K. Susceptibility data were obtained in applied fields of 10 kG. In addition, field sweeps were recorded at 5 K for $Eu_4K_2Na_2Ta_2O_{13}$. The very small diamagnetic contribution of the gelatin capsule containing the sample had a negligible contribution to the overall magnetization, which was dominated by the sample signal.

Photoluminescence. Emission and excitation spectra of $Eu_4Na_2K_2M_2O_{13}$ (M = Nb, Ta) were obtained using a PerkinElmer LS 55 Fluorescence Spectrometer using an excitation wavelength of 280 nm and emission wavelength of 610 nm, 290 nm and 610 nm for M = Nb and M = Ta, respectively. All measurements were performed at room temperature using ground crystals of $Eu_4Na_2K_2M_2O_{13}$. The compositions containing Nd, Sm, and Gd did not visibly luminesce and, therefore, their luminescence was not further investigated.

Results and Discussion

Crystal Structure. Molten alkali hydroxides are known to be an excellent medium for synthesizing single crystals of lanthanide containing complex oxides.[25,27,31] In the case of $Ln_4Na_2K_2M_2O_{13}$ (M = Nb, Ta; Ln = Nd, Sm, Eu, Gd), the Lux−Flood basic melt acted as both reactant and solvent. Although early transition metal oxides are reported to be more soluble in acidic hydroxide fluxes,[13,23] the title compounds are only accessible if open reaction vessels are used to allow for evaporation of water to dry the melt which, concomitantly, makes the melt more basic.

All compounds of the series $Ln_4Na_2K_2M_2O_{13}$ crystallize in the space group $C2/c$. Two schematics of the structure, which was reported previously,[21] viewed along the y-axis are shown in Figures 1 and 2. The crystal structure is best described by comparison with the structure of

Table 6. Selected Interatomic Distances (Å) for $Ln_4Na_2K_2Ta_2O_{13}$

	$Sm_4K_2Na_2Ta_2O_{13}$	$Eu_4K_2Na_2Ta_2O_{13}$
Ln(1)−O(1)	2.452(5)	2.439(5)
Ln(1)−O(2)	2.454(5)	2.445(5)
Ln(1)−O(3)^{iii}	2.428(5)	2.413(5)
Ln(1)−O(5)^{ii}	2.401(4)	2.389(3)
Ln(1)−O(6)	2.405(5)	2.397(4)
Ln(1)−O(7)	2.372(5)	2.351(5)
Ln(1)−O(7)^{i}	2.356(5)	2.349(5)
Ln(2)−O(1)^{iii}	2.383(5)	2.373(5)
Ln(2)−O(2)^{ii}	2.575(5)	2.560(5)
Ln(2)−O(3)	2.427(5)	2.410(5)
Ln(2)−O(5)	2.365(4)	2.356(3)
Ln(2)−O(6)^{vii}	2.415(5)	2.407(5)
Ln(2)−O(7)^{iii}	2.347(5)	2.339(5)
Ln(2)−O(7)^{vi}	2.373(5)	2.362(5)
Ta(1)−O(1)	1.981(5)	1.975(5)
Ta(1)−O(2)^{viii}	1.948(5)	1.952(4)
Ta(1)−O(3)^{iii}	1.939(5)	1.937(5)
Ta(1)−O(4)	1.831(5)	1.831(5)
Ta(1)−O(6)^{viii}	1.955(5)	1.951(4)
K(1)−O(1)	3.138(5)	3.139(5)
K(1)−O(1)^{iii}	3.252(5)	3.253(5)
K(1)−O(2)	3.118(5)	3.127(5)
K(1)−O(2)^{ii}	3.119(5)	3.112(5)
K(1)−O(3)	3.238(5)	3.242(5)
K(1)−O(3)^{iii}	3.197(5)	3.207(5)
K(1)−O(4)	2.900(6)	2.889(5)
K(1)−O(4)^{iii}	2.813(6)	2.806(5)
K(1)−O(4)^{iv}	2.828(6)	2.825(5)
K(1)−O(4)^{v}	2.932(6)	2.921(5)
Na(1)−O(1)^{iii}	2.276(6)	2.272(5)
Na(1)−O(2)^{iii}	2.309(6)	2.301(5)
Na(1)−O(3)	2.306(6)	2.302(5)
Na(1)−O(4)	2.294(6)	2.291(6)
Na(1)−O(6)^{v}	2.321(6)	2.320(5)

^{i}Symmetry code: $-x+1,-y,-z+1$ ^{ii}Symmetry code: $-x+1/2,-y+1/2,-z+1$ ^{iii}Symmetry code: $-x+1/2,y-1/2,-z+1/2$ ^{iv}Symmetry code: $x,-y,z+1/2$ ^{v}Symmetry code: $-x+1/2,y+1/2,-z+1/2$ ^{vi}Symmetry code: $x-1/2,-y+1/2,z-1/2$ ^{vii}Symmetry code: $-x+1/2,-y-1/2,-z+1$ ^{viii}Symmetry code: $x,-y,z-1/2$.

LnKNaMO$_5$.[19,20,24] The title compounds consist of a 2D-framework of double-layered Ln_4O_{11} polyhedra, in which the lanthanide atoms are coordinated by seven oxygen atoms, forming distorted "cubes" with one corner missing. Considering that one of the Ln−O bonds is significantly shorter than the other six, these polyhedra could also be described as distorted monocapped octahedra. Every polyhedron shares four of its edges with polyhedra in the same slab and three of its corners with three other lanthanide polyhedra belonging to the adjacent slab of the Ln_4O_{11} double layer. The structure is very similar to that of LnKNaMO$_5$, which, by contrast, is constructed of LnO$_4$ single layers in which the rare earth atom possesses a cubic 8-fold coordination environment.

The niobium and tantalum atoms in $Ln_4Na_2K_2M_2O_{13}$ are 5-fold coordinated, as they are in LnKNaMO$_5$; however, unlike in this latter structure where the NbO_5 square pyramids are regular in shape and only contain a shortened bond to the apical oxygen atom, the bases of the MO_5 pyramids in $Ln_4Na_2K_2M_2O_{13}$ are strongly distorted. This distortion originates in the Ln_4O_{11} double layer, which contains distorted Ln−O pseudo-cubes, to which the square pyramids are connected.

The sodium atoms are located in a coordination environment similar to that of niobium. Analogous to the structure of LnKNaMO$_5$, the MO_5 and NaO_5 pyramids

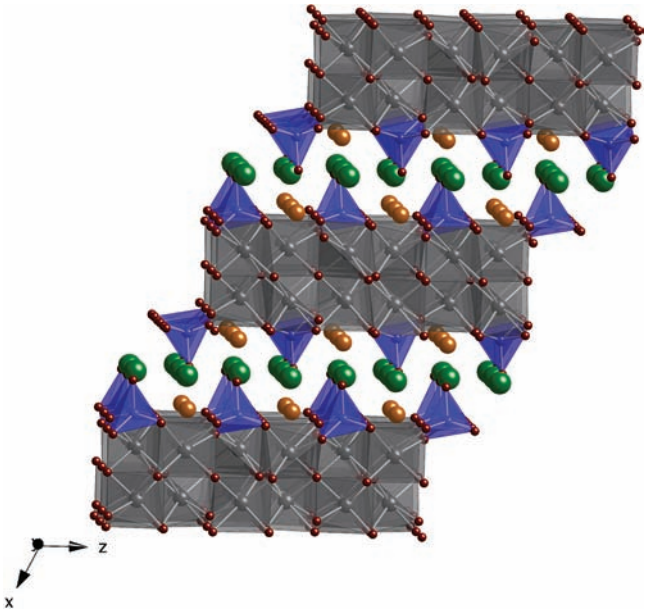

Figure 1. Schematic of the crystal structure of $Ln_4K_2Na_2M_2O_{13}$ viewed along the y-axis. NbO_5 polyhedra are shown in blue, LnO_7 polyhedra are shown in gray. The potassium and sodium atoms are represented as large green and orange spheres, respectively, and oxygen atoms as small red spheres.

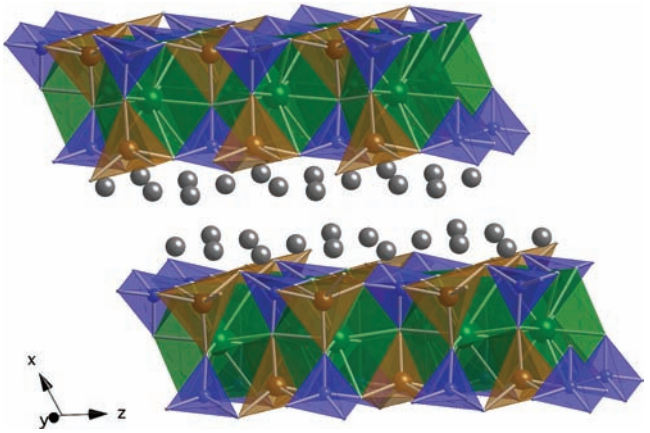

Figure 2. Schematic of the Crystal Structure of $Ln_4K_2Na_2M_2O_{13}$ viewed along the y-axis. NbO_5 polyhedra are shown in blue, NaO_5 and KO_{10} polyhedra in orange and green, respectively. Rare earth atoms are represented as gray spheres.

reside in alternating rows above the cavities formed by the Ln_4O_{11} framework. Each MO_5 pyramid shares its apical oxygen with one NaO_5 pyramid situated above the adjacent Ln_4O_{11} double layer, forming MNaO$_9$ apically linked square pyramidal double units. The potassium atoms are located in a 10-fold coordination environment with four oxygen atoms from the apexes of adjacent MO_5 pyramids and the other six residing on corners of cavities in the Ln_4O_{11} framework. By comparison, the potassium atoms in LaKNaNbO$_5$ possess 12-fold oxygen coordination. This difference is due to the reduced coordination environment of the rare earth cation in $Ln_4Na_2K_2M_2O_{13}$.

Stability Limits. It is of interest to compare the compositional stability limits of the $Ln_4Na_2K_2M_2O_{13}$ family of compounds with that of the LnKNaNbO$_5$[19] family.

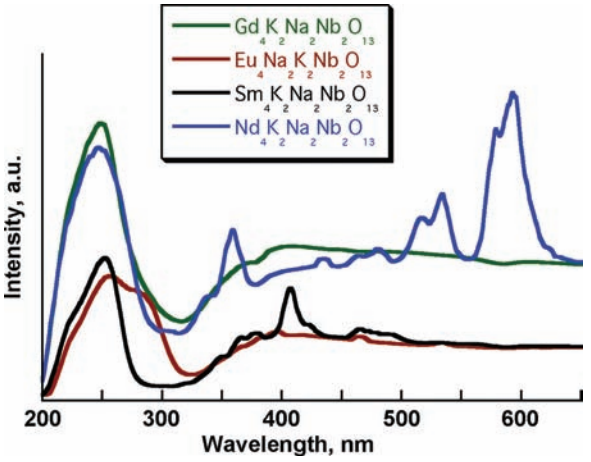

Figure 3. UV−vis diffuse-reflectance spectra of $Ln_4K_2Na_2Nb_2O_{13}$ at room temperature.

A significant structural difference is that in the *Ln*KNaNbO$_5$ family the rare earths are found in 8-fold coordination environments, while in the $Ln_4Na_2K_2M_2O_{13}$ family of compounds the rare earths are only 7-coordinate. As is well-known, the size and hence coordination number preference of the lanthanides decreases from lanthanum to lutetium. The early lanthanides prefer higher coordination numbers than the later ones, and their ionic radii are larger. Thus the different coordination environment should, and does, result in different rare earths being accommodated in the two different structure types. In the *Ln*KNaNbO$_5$ family, rare earths from lanthanum to terbium can be accommodated and the stability limit occurs at the terbium analog. No rare earth smaller than terbium can be accommodated by the structure. By contrast, the $Ln_4Na_2K_2M_2O_{13}$ family can accommodate rare earths from neodymium to gadolinium (niobium) and samarium to gadolinium (tantalum). No rare earth larger than neodymium or smaller than gadolinium can be accommodated.

Clearly, in both families of oxides, the rare earth coordination environment is important in determining which rare earths can be accommodated in these structure types. A look at the valence bond sums, Supporting Information, Table S1, however, does not show a compelling reason for a compositional limit. Similarly, in the *Ln*KNaNbO$_5$ family,[19] comparable valence bond sums for niobium and the rare earths were obtained and, there also, the valence bond sums did not reveal a compelling reason for a structural limit. We can only conclude that as the rare earth cations become smaller the preference for the lower 6-fold coordination environment eventually dominates, and the structures cease to form with these rare earths.

Magnetism. The magnetic susceptibilities of $Ln_4Na_2K_2M_2O_{13}$ (M = Nb, Ta; Ln = Nd, Sm, Eu, Gd) were measured over the temperature range 5−300 K in an applied field of 10 kG. The magnetic susceptibility of $Nd_4Na_2K_2Nb_2O_{13}$ suggests an onset of magnetic coupling at 25 K ($\mu_{eff} = 6.76$, $\mu_{calc} = 7.24$, $\theta = -36.4$ K); however, none of the other compositions show similar behavior and their magnetic moments are what is expected for non-interacting rare earth cations, Gd−Nb, $\mu_{eff} = 15.7$, $\mu_{calc} = 15.9$; Gd−Ta, $\mu_{eff} = 15.8$, $\mu_{calc} = 15.9$; Eu−Nb (300 K), $\mu_{eff} = 7.3$, $\mu_{lit} = 6.8$;[35] Eu−Ta (300 K), $\mu_{eff} = 6.7$, $\mu_{lit} = 6.8$;[35] Sm−Nb (300 K), $\mu_{eff} = 2.7$, $\mu_{lit} = 3$;[35] Sm−Ta (300), $\mu_{eff} = 2.7$, $\mu_{lit} = 3$;[35] (Supporting Information, Figures S1−S6).

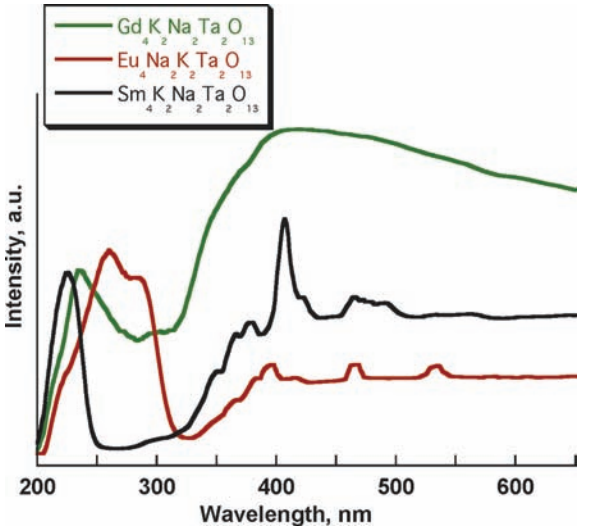

Figure 4. UV−vis diffuse-reflectance spectra of $Ln_4K_2Na_2Ta_2O_{13}$ at room temperature.

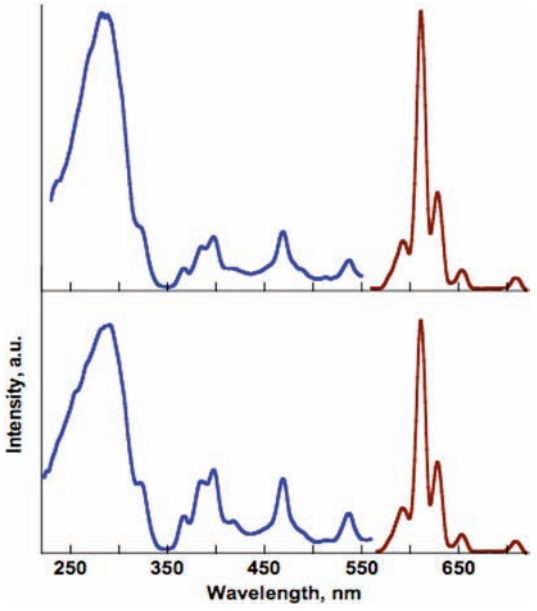

Figure 5. Room temperature photoluminescence spectra of $Eu_4K_2Na_2Nb_2O_{13}$ (on top) and $Eu_4K_2Na_2Ta_2O_{13}$ (on the bottom). Excitation spectra are shown in blue, emission spectra in red.

UV−vis Spectra. Diffuse-reflectance spectra were collected using ground crystals of $Ln_4Na_2K_2M_2O_{13}$ (Ln = Nd, Sm, Eu, Gd: M = Nb; Ln = Sm, Eu, Gd: M = Ta) and are shown in Figures 3 and 4. The oxides have a clearly visible absorption edge in the UV, corresponding to the energy gap between the valence band formed mostly by oxygen 2p orbitals and the empty conduction band formed to a large part by the metal d orbitals. Band gaps are estimated from the onset of the absorption-edge

(34) Hui, Y. Y.; Lin, C.-F. *Mater. Lett.* **2007**, *61*, 3802–3804.

(35) Kittel, C. *Introduction to Solid State Physics*, 5th ed.; John Wiley & Sons: New York, 1976.

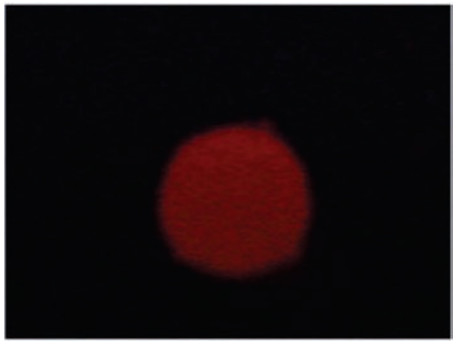

Figure 6. Optical image of $Eu_4K_2Na_2Nb_2O_{13}$ under UV-light irradiation.

position and fall into the 3.9 to 4.7 eV range, consistent with a wide band gap semiconductor. In addition, localized f-f transitions, because of the presence of the rare earth elements, can be seen in the visible portion of the spectra. These impart color to the samples; however, they play only a lesser role in the size of the band gap in these structures.

Photoluminescence. Figure 5 shows room temperature excitation and emission spectra of colorless $Eu_4Na_2K_2M_2O_{13}$ (M = Nb, Ta). For illustration purposes, Figure 6 provides an optical image of ground crystals of $Eu_4Na_2K_2Nb_2O_{13}$ under UV-irradiation. When exposed to short wavelength UV radiation, both compounds emit intense red light as seen in the optical picture. The emission spectra of both compounds have their maximum at 610 nm whereas the maximum of the excitation spectrum lies at 280 nm for the niobium compound and at 290 nm for the tantalum compound. All observed emission peaks in both spectra correspond to the $^5D_0 \rightarrow {}^7F_J$ (J = 1, 2, 3, 4) transitions of Eu^{3+}, which are mainly contributed by the rare earth's localized 4f energy levels. The two most intense peaks at 611 and 628 nm are attributed to the $^5D_0 \rightarrow {}^7F_2$ transition. It is well-known that the detailed spectral structure and the intensity of the emission peaks is strongly dependent on the symmetry of the crystal field around the europium ion.[14,34] The low symmetry environment around the rare earth cations in this structure increases the intensity of the $\Delta J = 2$ electric dipole transition relative to a high symmetry environment, greatly contributing to the intense red emission. The other observed emission peaks are at 591, 653, and 709 nm corresponding to the transitions $^5D_0 \rightarrow {}^7F_1$, $^5D_0 \rightarrow {}^7F_3$, and $^5D_0 \rightarrow {}^7F_4$, respectively.

It would be of interest to carry out detailed calculations in the future to establish the relationship between the crystal structure and the optical properties, as well as to generate a more detailed band structure.

Conclusion

Single crystals of seven different compositions of a new series of complex lanthanide oxides, $Ln_4Na_2K_2M_2O_{13}$ (Ln = Nd, Sm, Eu, Gd; M = Nb, Ta), were grown out of an alkali hydroxide flux. All compounds adopt a monoclinic structure in which the niobium or tantalum atoms are found in an unusual 5-fold coordination environment. UV−vis measurements revealed band gaps consistent with wide band gap semiconductors. The europium containing compounds were observed to exhibit intense room temperature photoluminescence. All emission peaks are attributed to the $^5D_0 \rightarrow {}^7F_J$ (J = 1, 2, 3, 4) transitions of Eu^{3+}.

Acknowledgment. This work was supported by the National Science Foundation through Grants DMR: 0450103 and DMR:0804209.

Supporting Information Available: Further details of the crystal structure investigations can be obtained from the Fachinformationszentrum Karlsruhe, 76344 Eggenstein-Leopoldshafen, Germany; fax: +49 7247 808 666; E-mail: crysdata@FIZ-Karlsruhe.de on quoting the depository numbers CSD-380309, CSD-380306, CSD-380308, CSD-380307, CSD-380311, CSD-380310, for $Nd_4K_2Na_2Nb_2O_{13}$, $Sm_4K_2Na_2Nb_2O_{13}$, $Eu_4K_2Na_2Nb_2O_{13}$, $Gd_4K_2Na_2Nb_2O_{13}$, $Sm_4K_2Na_2Ta_2O_{13}$, and $Eu_4K_2Na_2Ta_2O_{13}$, respectively. This material is available free of charge via the Internet at http://pubs.acs.org.